Improved Configuration of Halbach Magnets with a Homogeneous Magnetic Field for Portable NMR Device

Yi-Yuan Cheng [1], Ming-Yang Su [2], Tao Hai [1], Ming Hui[3], Bao-lei Li [3], and Ling Xia [4]

[1] Department of Mechanical and Electrical Engineering
Nanyang Normal University, Nanyang, 473061, China
chengyy850@gmail.com, nytcht@163.com

[2] Department of Environmental Engineering
Henan Polytechnic Institute, Nanyang, 473000, China
sumingyang@foxmail.com

[3] Department of Physics and Electrical Engineering
Nanyang Normal University, Nanyang, 473061, China
huimingsn@163.com, bl_li@qq.com

[4] Department of Biomedical Engineering
Zhejiang University, Hangzhou, 310027, China
xialing@zju.edu.cn

Abstract ─ Halbach array magnets are widely used in portable nuclear magnetic resonance (NMR) devices that the homogeneity of the magnetic field generated by the array affects the imaging quality. In this paper, we propose some improvements to the construction of the Halbach magnets to enhance magnetic field uniformity. Using a Halbach array model comprising 16 magnets, all the calculations are based on 3D finite element method (FEM) analysis and optimized using the particle swarm optimization (PSO) algorithm. Comparisons of the results are shown to support the observations that the optimized and improved constructions can generate a more homogeneous magnetic field.

Index Terms ─ Halbach magnet, improved configuration, particle swarm optimization, portable NMR.

I. INTRODUCTION

Portable nuclear magnetic resonance (NMR) devices have been of interest since the early 1950s for well-logging [1]. With the development of permanent magnet materials such as Nd–Fe–B in the 1990s, new prospects have emerged for portable NMR applications [2]. The first portable magnetic resonance imaging (MRI) system was proposed for mouse studies in 1995 [3]. Portable NMR devices must be relatively small in size and light in weight, so most devices use permanent magnets instead of superconducting magnets, which generate relatively low magnetic field strengths but can be used in outdoor environments and offer numerous applications.

Halbach magnets are widely used in portable NMR systems and were first proposed by Klaus Halbach for high-energy accelerators [4]; they have also been used in other electromagnetic systems, such as motors, eddy current brakes, and mobile MRI units [5-9]. Halbach magnets have several advantages [10-11]: First, these magnets are composed of small permanent magnet blocks that generate strong and homogeneous fields. Second, they produce a transverse magnetic field distribution in an air gap, which allows the usage of solenoid coils for NMR applications. Moreover, the stray field is small, and the magnets can be produced easily and economically. In particular, Halbach magnets satisfy several of the requirements of portable NMR devices and can be widely used [12].

The Halbach magnet generates a static magnetic field that largely determines the final imaging quality. The ideal Halbach magnet is theoretically expected to provide a homogeneous field, but the inhomogeneities are unavoidable. In this study, we consider some improved constructions for the Halbach magnet array to produce a homogeneous magnetic field. The simulation model comprises an array of 16 magnets, and all calculations are based on 3D finite element method (FEM) analysis.

To obtain a more homogeneous magnetic field, the proposed method improves the construction of the Halbach magnet array and optimizes it. The optimization procedure is a nonlinear and nonconvex problem with

Submitted On: October 17, 2019
Accepted On: May 20, 2021

https://doi.org/10.47037/2020.ACES.J.360509

multipole points owing to the nonlinear characteristics of the ferromagnetic materials. The conventional optimization methods generally converge at local optima and may be suitable for convex problems with single extreme points, where it is difficult to find the global optima in the optimization problems of electromagnetic fields. Particle swarm optimization (PSO) [13] proposed by Eberhart and Kennedy in 1995 is used to optimize the improved construction of the Halbach array in this work; PSO is one of the recently developed intelligent global optimization methods that can handle many complex optimization problems in engineering and science [14-15].

II. THEORY AND MODEL

A. Theory

The ideal Halbach magnet array is also known as a magic ring and is an infinite long hollow cylinder made of a permanent magnet material; the magnetization characteristics change regularly and continuously along the cylinder. The ideal and homogeneous magnetic field inside the hollow cylinder is as shown in Fig. 1 (a). The magnetic field intensity B_0 [16] inside the ideal Halbach magnet array can be defined as:

$$B_x = B_r \ln \frac{r_{outer}}{r_{inner}},\ B_y \cong 0,\ B_z \cong 0, \tag{1}$$

where B_r is the remanence of the magnetic material, and r_{outer} and r_{inner} are the outer and inner radii of the cylindrical magnet. In the ideal state, the magnetic field components in the y- and z-directions can be considered to be approximately 0.

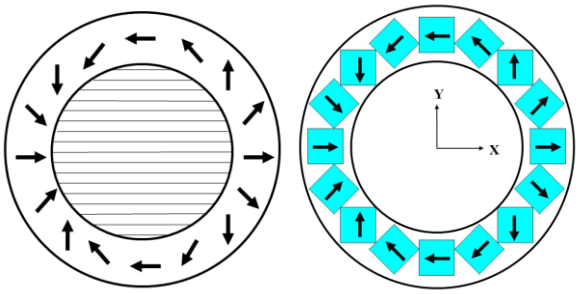

(a) (b)

Fig. 1. (a) Ideal halbach magnet; (b) mandhalas ring magnet.

In reality, the magnetization characteristics cannot change regularly and continuously along the cylinder, and the length of the magnet cannot be infinite; thus, inhomogeneities in the magnetic field cannot be avoided, which may influence the NMR image quality. Several Halbach array magnets made using discrete magnet blocks have been proposed and produced based on the theory of the ideal Halbach magnet. NMR-mandhalas [10], i.e., magnet arrangements for novel discrete Halbach layout, which are ring magnets, were proposed by Raich and Blumler in 2004, as shown in Fig. 1 (b); this structure is composed of 16 magnet blocks with the same sizes and magnetization characteristics. In this work, the 16-mandhalas ring magnet is used as the model for optimization.

The detailed theoretical description of the Halbach magnet array is as follows [8, 10, 17]. The Halbach magnet consists of permanent magnets with equal magnetizations that are oriented and positioned according to the analytic equations given below. There are two predetermined parameters for the exact geometry of the magnet arrangement: radius of the ring, r, and number of magnets, n. The position of each magnet is determined by its center (^cP_i), which is at a distance r from the origin, as shown in Fig. 2.

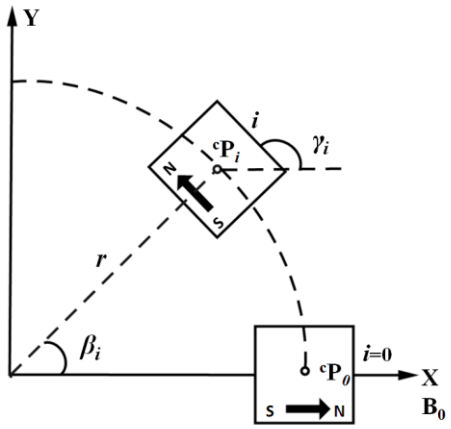

Fig. 2. Geometry of magnet coordinates.

The coordinates of the magnet centers are given as:

$$^cP_i = \begin{pmatrix} ^cx_i \\ ^cy_i \end{pmatrix} = r \begin{pmatrix} \sin\beta_i \\ \cos\beta_i \end{pmatrix}, \tag{2}$$

where $\beta_i = i\alpha$ for $i = 0, 1..., n\text{-}1$ and $\alpha = \frac{2\pi}{n}$.

Once the n magnets are spatially arranged, their size a is scaled such that the densest possible arrangement can be obtained. This results in the following coordinates for the corners of the i-th magnet:

$$\begin{aligned}
^1P_i &= \begin{pmatrix} ^1x_i \\ ^1y_i \end{pmatrix} = ^cP_i + \frac{a}{\sqrt{2}} \begin{pmatrix} \cos\xi_i \\ \sin\xi_i \end{pmatrix} \\
^2P_i &= \begin{pmatrix} ^2x_i \\ ^2y_i \end{pmatrix} = ^cP_i + \frac{a}{\sqrt{2}} \begin{pmatrix} -\sin\xi_i \\ \cos\xi_i \end{pmatrix} \\
^3P_i &= \begin{pmatrix} ^3x_i \\ ^3y_i \end{pmatrix} = ^cP_i + \frac{a}{\sqrt{2}} \begin{pmatrix} -\cos\xi_i \\ -\sin\xi_i \end{pmatrix} \\
^4P_i &= \begin{pmatrix} ^4x_i \\ ^4y_i \end{pmatrix} = ^cP_i + \frac{a}{\sqrt{2}} \begin{pmatrix} \sin\xi_i \\ -\cos\xi_i \end{pmatrix}
\end{aligned}, \tag{3}$$

where $\xi_i = \frac{\pi}{4} - 2\beta_i$.

From the above equations, we can determine the position and arrangement of each magnet, as shown in Fig. 3.

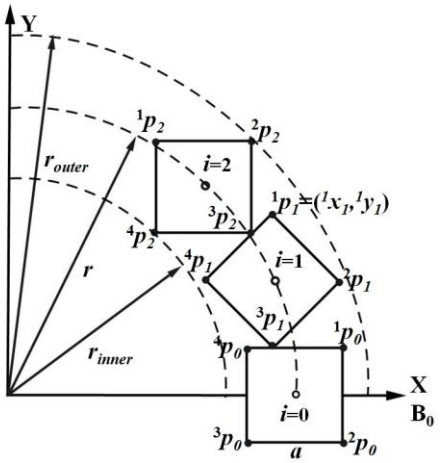

Fig. 3. Schematic representation of the magnet coordinates.

The magnet size, *a*, is given by:

$$a = 2r\Xi(\alpha), \tag{4}$$

where $\Xi(\alpha) = \dfrac{\cos\alpha - \sin\partial - \sqrt{2}\sin\left(\frac{\pi}{4} - 2\alpha\right)}{2\cos\left(\frac{\pi}{4} - 2\alpha\right) + \sqrt{2}}$.

The inner and outer radii are given by:

$$r_{inner} = r\left(1 - \sqrt{2}\Xi(\alpha)\right), \tag{5}$$

$$r_{outer} = r\left(1 + \sqrt{2}\Xi(\alpha)\right). \tag{6}$$

B. Initial Halbach array magnet model

Based on the above theory, we build the initial 3D half-Halbach array model with n = 16 magnet blocks of dimensions 22.2×22.2×200 mm^3. The radius is r = 70 mm, inner radius is r_{inner} = 54.3 mm, and outer radius is r_{outer} = 85.7 mm. The model is shown in Fig. 4, and each magnet is numbered consecutively for later use. The black arrows represent the direction of magnetization. The magnets are made from Nd–Fe–B (N40) permanent magnet material with a coercivity of 939,014.18 A/m and relative permeability of 1.085, assuming linear dependence between B and H. The orientation of the magnetic field, which unlike those of traditional superconducting magnets is perpendicular to the ring axis, defines the x-direction of the proposed reference system, while the z-axis is directed along the bore.

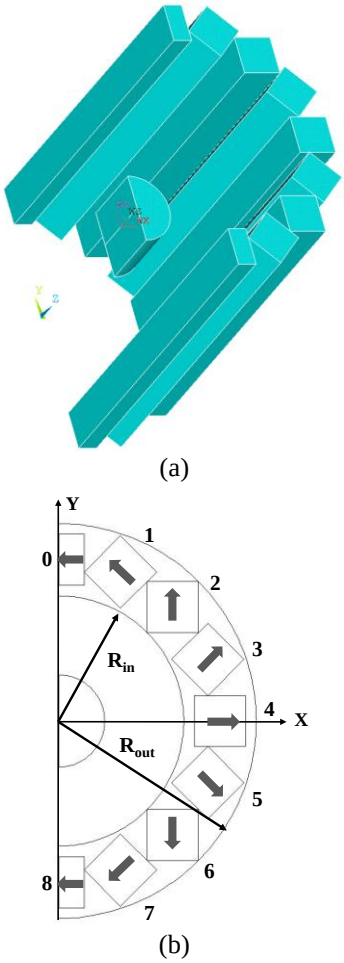

Fig. 4. 3D model (a) initial half; (b) cross section.

In the design of the magnet, we focused on high field homogeneity for the central part of the magnet, with a cylindrical volume of 20 mm diameter and 20 mm length. The field uniformity U is defined as:

$$U = \frac{B_{\max} - B_{\min}}{B_{avg}}, \tag{7}$$

where B_{min}, B_{max}, and B_{avg} are the respective minimum, maximum, and averaged magnetic flux densities of the grid elements in a cylindrical volume of 20 mm diameter and 20 mm length in the FEM calculations.

The 3D FEM analysis of the permanent magnet was carried out using ANSYS 14.0 (www.ansys.com) software, and a half model is considered here because of the symmetry of the model. The conditions of the air-field boundary in a long distance are set to zero flux, for a distance that is five times the height and the outer radius of the entire magnet. We choose the solid 117 type element in ANSYS for the edge-based FEM. The model is divided using a free tetrahedral mesh. Based on practical experience with meshing, to ensure reliability of calculations, the components of concern or

components with larger changes in the magnetic fields need be divided into smaller grids [18]; hence, a fine mesh is used in the center cylindrical imaging region. The magnets are divided into larger grids in regions other than the center imaging region, and the external air part is meshed using a slightly coarse grid.

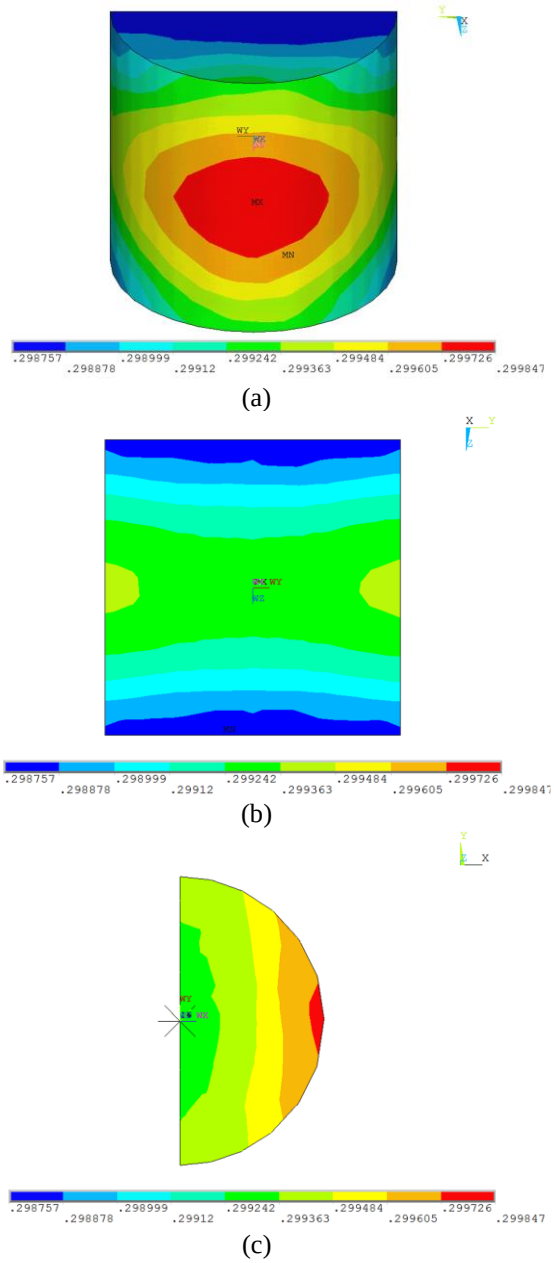

Fig. 5. The magnetic field distribution of the initial model: (a) the cylindrical volume; (b) the yz plane (x=0); (c) the xy plane (z=0).

For the initial model, a magnetic flux density of 0.2998 T and a field uniformity of 3393.88 parts per million (ppm; 10^{-6}) are obtained through ANSYS. Figure 5 shows the magnetic field distribution of the cylindrical volume at the center of the magnet. The homogeneity of the magnetic field at the imaging center is very important for ensuring good imaging quality, so an effective method should be used to improve the magnetic field in the initial magnet model.

III. IMPROVED CONFIGURATIONS

Based on the 2D simulation models reported in a previous work [19], two improved 2D constructions of Halbach magnet using PSO algorithm have been proposed. We extend these methods from the 2D model to the 3D model in this work, namely method 1 and method 2, as follows. The 2D models are based on the assumption that the z-direction is infinite; however, as the magnet has finite length with complex considerations in the 3D model, weaker magnetic fields may be observed at the ends of the cylindrical volume. The other methods will be taken into consideration for the finite length，such as stack structure, addition of shim units and so on.

A. Method 1: Changes to the sizes of the magnets

In theory, all the magnets are of the same size and have similar magnetization characteristics. If we change the sizes of some of the magnets, the magnetic field at the center will be changed. Because most of the magnets are rotated at a theoretical angle, we only consider magnets 0, 4, and 8, whose positions can be easily controlled, as shown in Fig. 6 (a); the additional parts are made of the same magnetic material as the original magnets. The magnet on the right has an increased thickness of W1, and the top and bottom magnets have thicknesses increased by W2. The values of W1 and W2 are obtained by optimization later.

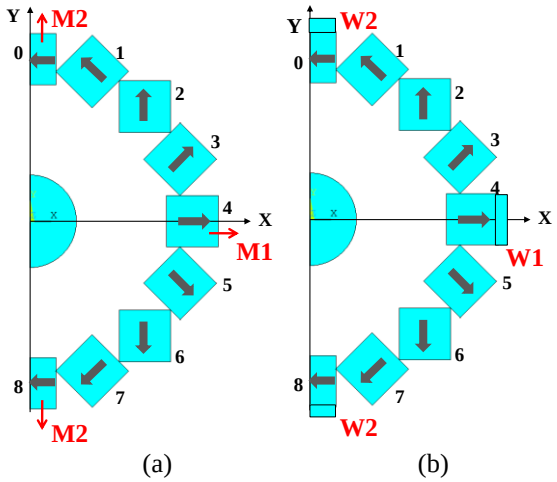

Fig. 6. Schematic cross section of: (a) changing the size of the magnets; (b) moving the position of the magnet towards outside.

B. Method 2: Moving the positions of the magnets

In another paper [12], it is noted that the "magic ring" is shifted outward by 5 mm from the center along the radius. If we want to change the magnetic field at the center, it can be achieved by moving the magnets outward or inward. Here, only the magnets numbered 0, 4, and 8 are considered as their positions can be easily controlled, as shown in Fig. 6 (b). A positive value of M1/M2 in Fig. 6 (b) implies moving outward, and a negative value implies moving inward. The values of M1 and M2 are determined by PSO, as shown later.

C. Method 3: Stack structure

The first two methods change only the radial distances of the magnets to improve the uniformity at the center of the magnetic field. However, when the model is extended to three dimensions, the axial direction must also be considered in addition to the radial direction. The most important problem with the 3D magnet model is that the imaging center has a weaker magnetic field at the ends but is stronger in the middle because of the finite length of the magnet. In a previous work [10], a stack structure also called as a "sandwich", was proposed comprising several short mandhala rings in the z-direction. The short mandhala rings are supported by an aluminum frame, with air gaps between the rings to ensure a more uniform magnetic field. Stacking more than six "magic rings" improves the field homogeneity within the stack but increases the weight and cost [20].

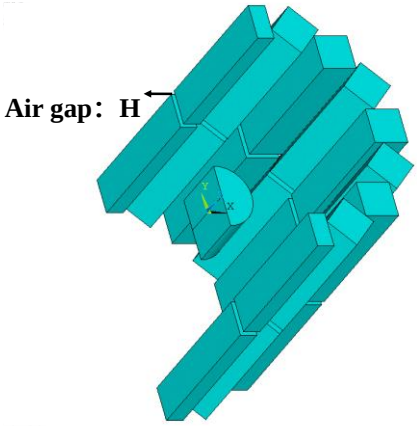

Fig. 7. Schematic representation of stack structure.

Considering the complexity of modeling, magnet weight, and manufacturing cost, we explore a two-ring stack structure where the magnet is divided into the upper and lower parts by an air gap of height H, as shown in Fig. 7. The stack structure can weaken the strength of the magnetic field in the middle, which will generate a more uniform field over the cylindrical volume.

D. Method 4: Addition of shim units

The weaker magnetic field at the ends of the magnet can be enhanced through adding some shim units to improve the uniformity of the center imaging volume. Two smaller rings with smaller magnets at the top and bottom of the cylinder are added to provide end-correction fields to offset the fall-off of the finite array in the z-direction [7, 21]. Because the magnet model used in this study is relatively small, we added eight shim units, four each at the top and bottom of the magnet. The positions of the four units are symmetrically distributed along the x and y axes, as shown in Fig. 8. The cross section of the shim unit is square, with a side length of 10 mm, height UAZ, and the positions (determined by DX and DY) optimized later. The material of the shim units is identical to that of the magnet, and the magnetization direction is same as those of the adjacent magnets.

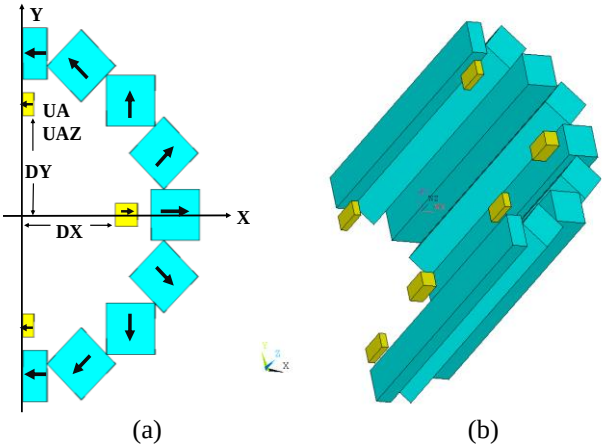

Fig. 8. Schematic representation of adding shim units: (a) cross-section; (b) half model.

E. Combination of several methods

The methods mentioned above are not mutually exclusive, so it is possible to optimize with a combination of these methods, e.g., combination of Methods 1 and 3, combination of Methods 2, 3, and 4. All the parameters in these methods can be optimized at the same time. By combining the optimizations of these methods, we hope to find a relatively optimal structure that can generate a uniform magnetic field in the imaging area.

IV. SIMULATION AND OPTIMIZATION

In this study, the 3D FEM analysis of permanent magnets is carried out using ANSYS (version 14.0, www.ansys.com). Owing to the symmetry of the magnet model, only a half model is considered. To obtain the homogeneous DSV, the parameters of the methods mentioned above are optimized using the PSO algorithm, which is programmed in MATLAB R2009b (The MathWorks, Natick, MA, USA). The optimized design parameters obtained by PSO are then used to calculate

the magnetic field of model. The optimized variables and constrains are listed in Table 1.

Table 1: Optimization variables and constraints

Methods	Optimization Variables	Constrains (mm)
Method 1: Change size	W1, W2	[0.2, 10]
Method 2: Move position	M1, M2	[-5, 5]
Method 3: Stack structure	H	[1, 5]
Method 4: Shim unit	DX, DY	[30, 45]
	UAZ	[5, 20]

In the PSO algorithm, we choose the uniformity of the cylindrical volume of 20 mm diameter and 20 mm length as the objective function and fitness of PSO. The optimization can be expressed as:

Minimize

$$U = \frac{B_{\max}\left(x_1, L, x_k\right) - B_{\min}\left(x_1, L, x_k\right)}{B_{avg}\left(x_1, L, x_k\right)}, \quad (8)$$

where x_1 to x_k are the optimization parameters or variables from the different methods listed in Table 1.

Based on the number of optimization parameters using the different methods, the population size of the PSO algorithm may differ. According to the rule that more parameters have a greater number of groups, the detailed population sizes of the different methods are shown in the Table 2 below. In addition, the number of iterations for the different methods is set to 100.

Table 2: Optimization parameters and population sizes

Methods	Optimized Parameters by PSO (mm)	Population Sizes
Method 1: Change size	W1, W2	20
Method 2: Move position	M1, M2	20
Method 4: Shim unit	DX, DY, UAZ	30
Method 1+3: Change size + Stack	W1, W2, H	30
Method 2+3: Move position + Stack	M1, M2, H	30
Method 3+4: Stack + Shim unit	DX, DY, UAZ, H	40
Method 1+3+4: Change size+Stack+Shim unit	DX, DY, UAZ	30
Method 2+3+4: Move position+Stack+Shim unit	DX, DY, UAZ	30

V. RESULTS

A. Results of Method 1, Method 2, Method 3 and Method 4

We provide the results of Method 3, i.e., the stack structure first. There is only one parameter in Method 3, and we calculate the magnetic field values for air gap values of H = 1, 2, 3, 4, 5, and 6 mm; these results are shown in Fig. 9.

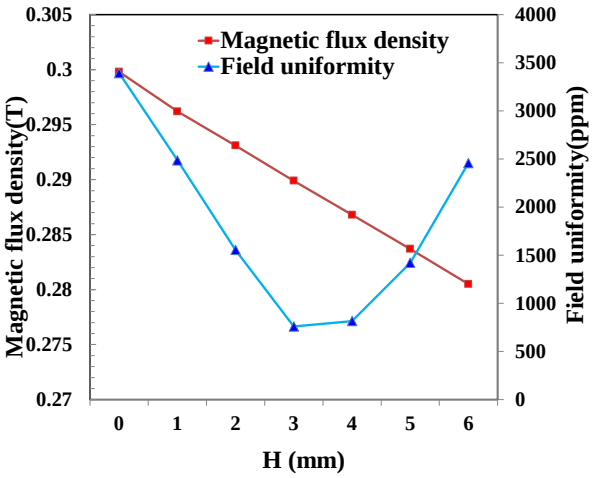

Fig. 9. The magnetic field with different air gaps in the stack structure.

The initial model with H = 0 mm is compared to the others. The strength of the magnetic field is weakened according to the increase in the gap height, and the uniformity is improved correspondingly; however, this air gap cannot be increased continuously. When the air gap is 3 mm, the magnetic field is most uniform, as shown in Fig. 10. These results show that the magnet with the stack structure can generate a more uniform magnetic field than the initial model, but the uniformity cannot meet the demands of imaging. We therefore combine the stack structure with other methods, and the optimization range of the air gap is restricted to the range of [1 mm, 5 mm] based on the results of optimization.

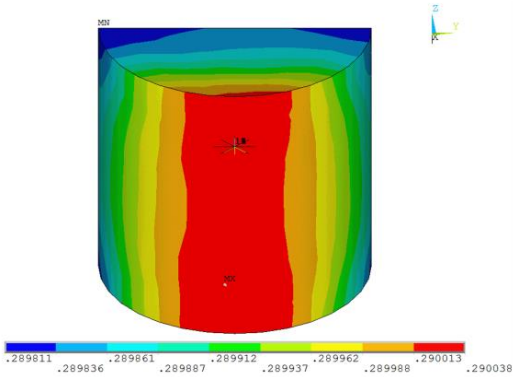

(a)

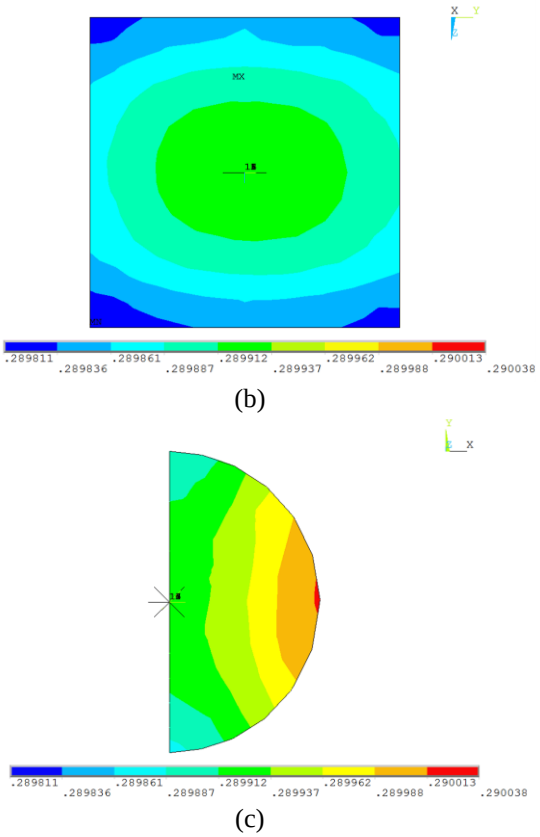

(b)

(c)

Fig. 10. The magnetic field distribution with H=3 mm air gap. (a) the cylindrical volume; (b) the yz plane (x=0); (c) the xy plane (z=0).

The parameters of Methods 1, 2, and 4 are optimized by iterative calculations of the PSO, and the comparisons are displayed in Table 3. From these results, we see that the uniformities of the obtained magnetic fields are much better than those when using the methods individually, especially in the combinations of Methods 1 and 2 with Method 3. The magnetic flux densities are observed to be weakened slightly owing to the air gap of the stack structure.

Table 3: Optimization results

Methods	Optimized Parameters by PSO (mm)	Magnetic Flux Density (T)	Field Uniformity (ppm)
Initial model	NULL	0.2988	3393.8817
Method 1: Change size	W1=1.7574 W2=6.5851	0.3077	2863.2789
Method 2: Move position	M1=-0.0221 M2=-3.8119	0.3063	2752.3956
Method 4: Shim unit	DX=42.6497 DY=33.6686 UAZ=19.8297	0.2998	2976.2469

B. Results of Methods 1+3, Methods 2+3, and Methods 3+4

The previous section presents the results of the four methods separately, and the uniformities of the magnetic field are marginally improved in each case. We therefore combine these methods for optimization, i.e., Method 3 with each of the other methods. Based on these combinations, an extra optimization parameter is added to Methods 1, 2, and 4, namely the height of the air gap, H, of the stack structure. After iterative calculation of the PSO, the obtained results are shown in Table 4.

Table 4: Optimization results

Methods	Optimized Parameters by PSO (mm)	Magnetic Flux Density (T)	Field Uniformity (ppm)
Initial half model	NULL	0.2988	3393.8817
Method 1+3: Change size + Stack	W1=2.0568 W2=4.2943 H=3.3908	0.2955	246.2565
Method 2+3: Move position + Stack	M1=-0.0532 M2=-1.2619 H=3.3229	0.2908	258.2889
Method 3+4: Stack + Shim unit	DX=35.8377 DY=36.9083 UAZ=19.3052 H=3.1307	0.2898	498.0765

C. Results of Methods 1+3+4 and Methods 2+3+4

Adding the shim units does not conflict with Methods 1+3 and 2+3; hence, we combined the addition of the shim units with the optimization models of Methods 1+3 and 2+3. The positions and heights of the shim units are optimized by PSO to obtain the final results shown in Table 5.

Table 5: Optimization results

Methods	Optimized Parameters by PSO (mm)	Magnetic Flux Density (T)	Field Uniformity (ppm)
Method 1+3+4: Change size+ Stack+Shim unit	DX=34.7569 DY=39.9797 UAZ=5.1494	0.2955	284.1458
Method 2+3+4: Move position+ Stack+Shim unit	DX=31.6021 DY=44.3450 UAZ=5.0169	0.2909	249.9071

From the results in Table 5, we can see that the magnetic field uniformity is not better but worse after adding the shim units, which is increased by about 40 ppm, so it's infeasible that adding the shim units to the improved configuration optimized by Method 1+3. Besides, the other improved configuration optimized by Method 2+3, generate a stronger and more uniform magnetic field after adding the shim units.

D. Comparisons of some results

(1) Comparisons of Weight

Beside the flux density and homogeneity, the mass of the magnet is an important design criterion, especially for portable applications. The density of the magnet material is known (Nd–Fe–B: $\rho = 7.5$ g·cm^{-3} as a reference), and we can estimate the weight of magnets roughly as a reference, as shown in Fig. 11. The weight estimations include only that of the permanent magnet material used in the model and not those of the support structures and other components used in the actual device.

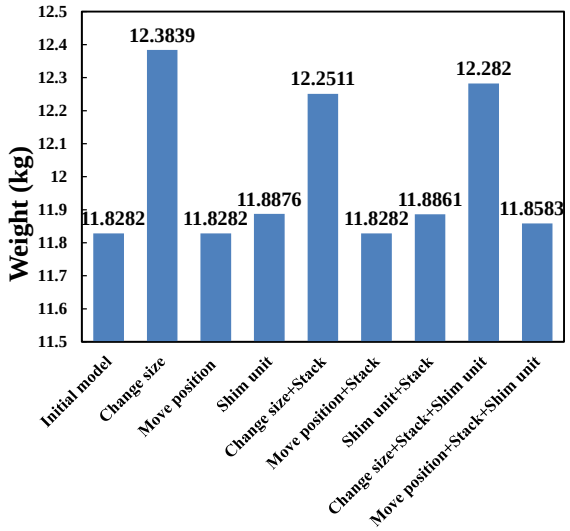

Fig. 11. Weight of the whole magnets model.

The weight of the permanent magnet material used in the initial whole magnet is about 11.8282 kg. Some methods do not change the weight of the magnet, such as the methods involving moving the position and the stack structure, because no extra material is added. However, weight increment is inevitable in the methods involving changing the size and adding the shim units; in particular, the weight increases more in the method of changing the size of the magnet (about 0.5 kg).

These calculations only consider the weight of the permanent magnet materials used in the model, but there are the mutual attractive and repulsive forces between the magnets in practice, so an external framework is needed to maintain the arrangement of the magnets. This framework must made of a light material, such as aluminum, to minimize the overall weight of the system.

(2) Comparisons of Three Combinations

Among the previous attempts at optimization, we choose the three most improved combinations of the Halbach magnet array that have better uniformities for imaging compared with the initial model. These are Methods 1+3, 2+3, and 2+3+4.

In the above work, we focused on the field density and uniformity in a cylindrical volume of 20 mm diameter and 20 mm length. Now, we calculate the magnetic field at the center of the ring for different cylindrical volumes. All these cylindrical volumes have the origin of the coordinate system as the center, and the diameters and heights are varied from 8 mm to 20 mm. We obtain the minimum, maximum, and average magnetic flux density from these calculations, and the statistical results are shown in Fig. 12.

The magnetic field of the initial model is as shown in Fig. 12 (a), and the average magnetic flux density is about 0.2993 T. The deviation over a small cylindrical volume is smaller, which means that the uniformity is better than that of a large cylindrical volume. The deviations over different cylindrical volumes are smaller for the three improved Halbach magnet arrays than those for the initial configuration, indicating that all three optimized methods generate more uniform magnetic fields. Compared to Fig. 12 (c), shim units are added in the configuration of Fig. 12 (d); thus, the average magnetic flux density increases.

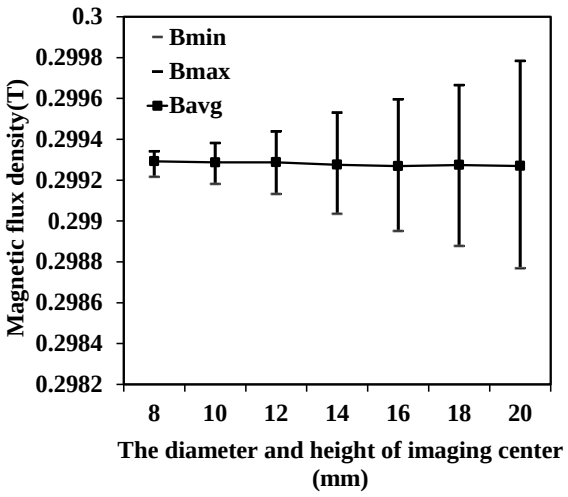

(a)

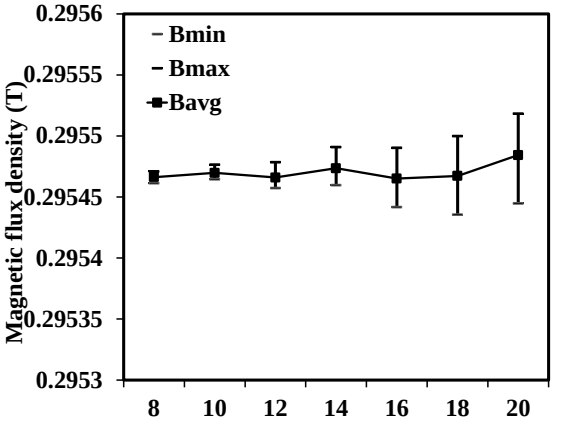

(b)

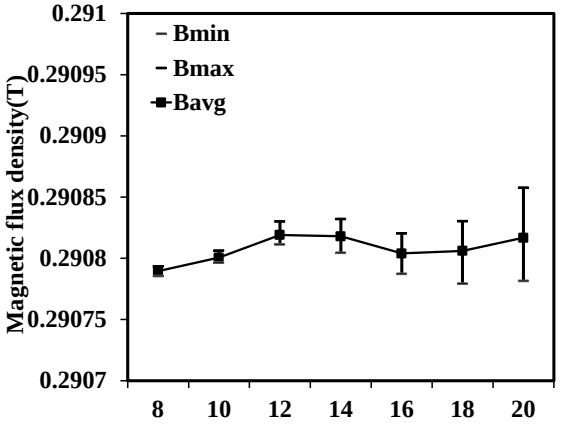

(c)

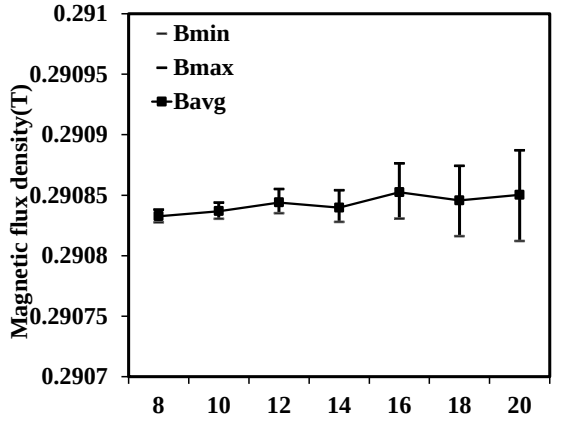

(d)

Fig. 12. The average magnetic flux density and standard deviation over different cylindrical volumes of the center imaging. (a) the initial model; (b) method 1+3: change size + stack; (c) method 2+3: move position + stack; (d) method 2+3+4: Move position + Stack + Shim unit.

There are no considerable differences among the three improved Halbach magnet arrays over different cylindrical volumes, as shown in Fig. 13. Here, we do not recommend the improved magnet with the shim units because the shim units involve uncertainties that affect the quality of the magnetic field, such as accuracies of location and size, magnetization characteristics, and so on. At the same time, the shim units occupy some of the inner space in the magnet, which will affect the arrangement of the gradient and radio frequency (RF) coils. In comparison, the other two improved Halbach magnet configurations have relatively simple structures and are recommended.

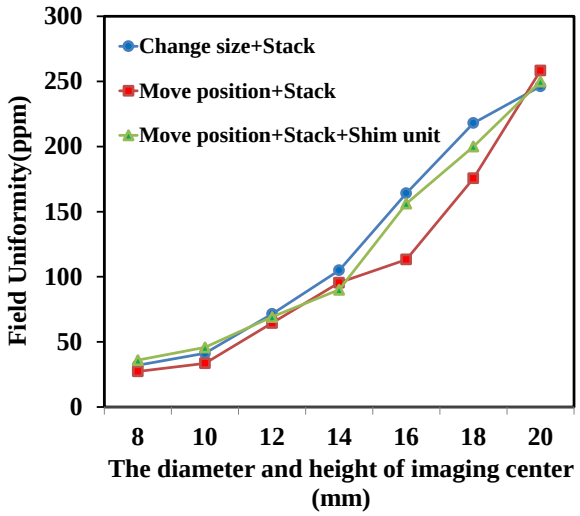

Fig. 13. The magnetic field uniformity over different cylindrical volumes.

VI. DISCUSSION AND CONCLUSION

In this study, a few different optimized configurations of the Halbach magnet array are proposed. Simulations were performed to validate the designs and show that the optimized constructions could significantly improve the magnetic field uniformity.

The design and optimization of the magnet are improved along the radial and axial directions at the same time. Method 1 involving changing the sizes of some of the magnets and Method 2 involving moving the positions of some of the magnets are extended from a 2D model to a 3D model along the radial direction. Method 3 involving the stack structure and Method 4 involving addition of shim units are based on the axial direction; hence, we combine these methods to obtain three improved configurations with low nonuniformities.

In the proposed optimized configurations, there are only two layers in the stack structure. More layers in the stack will generate more uniform magnetic fields, but these complex structures will have increased cost and more factors need to be controlled. Adding shim units should be carefully considered because the location and size as well as magnetization characteristics of the shim units might affect the accuracy of shimming directly. The design and simulations are based on improvement of configuration of the magnets that have more limitations, so shimming coils can be used for further improvement of the homogeneity, which is easier and more practical.

In future work, more comparisons can be performed using conventional optimization methods and PSO. In addition, improved configurations of the Halbach magnet array with homogeneous magnetic fields can be compared with other published results.

ACKNOWLEDGMENT

This work was supported in part by the National Natural Science Foundation of China under Grant No. 61701262, the scientific and technological project of Henan Province in China under Grant No. 182102310610, the key scientific research project in colleges of Henan Province in China under Grant No. 17A510016 and the special project of Nanyang Normal University in China under Grant No. ZX2016011.

REFERENCES

[1] D. E. Woessner, "The early days of NMR in the Southwest," *Concepts in Magnetic Resonance*, vol. 13, pp. 77-102, 2001.

[2] M. Sagawa, S. Fujimura, H. Yamamoto, Y. Matsuura, and K. Hiraga, "Permanent magnet materials based on the rare earth-iron-boron tetragonal compounds," *IEEE Transactions on Magnetics*, vol. 20, pp. 1584-1589, 1984.

[3] G. Eidmann, R. Savelsberg, P. Blümler, and B. Blümich, "The NMR MOUSE, a mobile universal surface explorer," *Journal of Magnetic Resonance*, Series A, vol. 122, pp. 104-109, 1996.

[4] K. Halbach, "Permanent magnets for production and use of high energy particle beams," *in Proceedings of the Eighth International Workshop on Rare Earth Cobalt Permanent Magnets and Their Applications*, Dayton, Ohio, pp. 103, May 1985.

[5] Z. Zhu and D. Howe, "Halbach permanent magnet machines and applications: A review," *IEE Proceedings-Electric Power Applications*, vol. 148, no. 4, pp. 299-308, 2001.

[6] W. Min, M. Zhang, Y. Zhu, B. Chen, G. Duan, J. Hu, and W. Yin, "Analysis and optimization of a new 2-D magnet array for planar motor," *IEEE Transactions on Magnetics*, vol. 46, pp. 1167-1171, 2010.

[7] E. Danieli, J. Mauler, J. Perlo, B. Blümich, and F. Casanova, "Mobile sensor for high resolution NMR spectroscopy and imaging," *Journal of Magnetic Resonance*, vol. 198, pp. 80-87, 2009.

[8] N. Doğan, R. Topkaya, H. Subaşi, Y. Yerli, and B. Rameev, "Development of Halbach magnet for portable NMR device," *Journal of Physics: Conference Series*, 153. 012047, 2009.

[9] C. W. Windt, H. Soltner, D. Dusschoten, and P. Blümler, "A portable Halbach magnet that can be opened and closed without force: The NMR-CUFF," *Journal of Magnetic Resonance*, vol. 208, pp. 27-33, 2011.

[10] H. Raich and P. Blümler, "Design and construction of a dipolar Halbach array with a homogeneous field from identical bar magnets: NMR Mandhalas," *Concepts in Magnetic Resonance Part B: Magnetic Resonance Engineering*, vol. 23, pp. 16-25, 2004.

[11] B. Hills, K. Wright, and D. Gillies, "A low-field, low-cost Halbach magnet array for open-access NMR," *Journal of Magnetic Resonance*, vol. 175, pp. 336-339, 2005.

[12] J. Chen and C. Xu, "An improved discrete configuration of a cylinder magnet for portable nuclear magnetic resonance instruments," *Journal of Applied Physics*, vol. 101, pp. 123926-123926, 2007.

[13] J. Kennedy and R. Eberhart, "Particle swarm optimization," *IEEE International Conference of Neural Networks*, Perth, Australia, pp. 1942-1948, 1995.

[14] M. AlRashidi and M. El-Hawary, "A survey of particle swarm optimization applications in electric power systems," *IEEE Trans. Evolutionary Computation*, vol. 13, pp. 913-918, 2009.

[15] J. Park, Y. Jeong, J. Shin, and K. Lee, "An improved particle swarm optimization for nonconvex economic dispatch problems," *IEEE Trans. Power Systems*, vol. 25, pp. 156-166, 2010.

[16] G. Moresi and R. Magin, "Miniature permanent magnet for table‐top NMR," *Concepts in Magnetic Resonance Part B: Magnetic Resonance Engineering*, vol. 19, pp. 35-43, 2003.

[17] H. Soltner and P. Blümler, "Dipolar Halbach magnet stacks made from identically shaped permanent magnets for magnetic resonance," *Concepts in Magnetic Resonance Part A*, vol. 36, pp. 211-222, 2010.

[18] Y. Y. Cheng, T. Hai, Y. B. Zheng, B. L. Li, and L. Xia, "Optimization and design of multi-ring pole pieces for small-sized permanent magnetic resonance imaging magnet," *Applied Computational Electromagnetics Society Journal*, vol. 33, no. 9, pp. 1026-1033, 2018.

[19] Y. Cheng, L. Xia, W. He, M. Zhu, and F. Liu, "Improved Halbach magnets by particle swarm optimization for mobile nuclear magnetic resonance systems," *in Ninth International Conference on Natural Computation, IEEE*, pp. 798-802, 2013.

[20] S. Anferova, V. Anferov, J. Arnold, E. Talnishnikh, M. A. Voda, K. Kupferschläger, P. Blümler, C. Clauser, and B. Blümich, "Improved Halbach sensor for NMR scanning of drill cores," *Magnetic resonance imaging*, vol. 25, pp. 474-480, 2007.

[21] C. Z. Cooley, J. P. Stockmann, B. D. Armstrong, M. Sarracanie, M. H. Lev, M. S. Rosen, and L. L. Wald, "Two‐dimensional imaging in a lightweight portable MRI scanner without gradient coils," *Magnetic Resonance in Medicine*, vol. 73, pp. 872-883, 2014.

Yi-Yuan Cheng was born in Henan, China, in 1985. She received her B.E. degree in Biomedical Engineering from South-Central University for Nationalities, Wuhan, China, in 2008, and received Ph.D. degree in Biomedical Engineering from Zhejiang University, Hangzhou, China, in 2015. She is currently working as a Lecturer in the Department of Mechanical and Electrical Engineering in Nanyang Normal University, Nanyang, China. Her main research interests include MRI, design and optimization of magnet, artificial intelligence and so on.

Ming-Yang Su was born in Henan, China, in 1984. He received his Bachelor degree of Engineering from Qingdao University of Science and Technology, Qingdao, China, in 2006 and Master degree from Qingdao University of Science and Technology in 2010. He is currently working as a Lecturer in Henan Polytechnic Institute, Nanyang, China. His main interests in materials research.

Tao Hai was born in Henan, China, in 1974. He received his Ph.D. degree in Signal and Information Processing from Harbin Engineering University, Harbin, China. He is currently working as a Lecturer in the Department of Mechanical and Electrical Engineering in Nanyang Normal University, Nanyang, China. His main research interests include signal processing, image processing and so on.

Ming Hui was born in Henan, China, in 1983. He received his Ph.D. degree in Communication and Information System from Ningbo University, Ningbo, China, in 2013. He is currently working as an Associate Professor in the Department of Physics and Electrical Engineering in Nanyang Normal University, Nanyang, China. His main research interests include the design of high efficiency RF power amplifier and the linearization technology.

Bao-Lei Li was born in Henan, China, in 1987. He received his Ph.D. degree in Information and Communication Engineering from Yunnan University, Kunming, China. He is currently working as a Lecturer in the Department of Physics and Electrical Engineering in Nanyang Normal University, Nanyang, China. His main research interests include intelligent optimization algorithm, path planning and so on.

Ling Xia was born in Zhejiang, China, in 1965. He received his B.E. degree in Automation and Ph.D. degree in Biomedical Engineering from Zhejiang University, Hangzhou, China. He is currently working as a Professor in the Department of Biomedical Engineering in Zhejiang University, Hangzhou, China. His main research interests include MRI key technical issues, biological effects of electromagnetic fields, Physiological simulation and modeling and so on.